Experimental Eye Research 92 (2011) 57–66

Contents lists available at ScienceDirect

Experimental Eye Research

journal homepage: www.elsevier.com/locate/yexer

A model of giant vacuole dynamics in human Schlemm's canal endothelial cells

Ryan M. Pedrigi [a], David Simon [b], Ashley Reed [b], W. Daniel Stamer [c], Darryl R. Overby [a,b,*]

[a] Department of Bioengineering, Imperial College London, London SW7 2AZ, UK
[b] Department of Biomedical Engineering, Tulane University, New Orleans, LA 70118, USA
[c] Department of Ophthalmology and Vision Science, University of Arizona, Tucson, AZ 85711, USA

ARTICLE INFO

Article history:
Received 3 July 2010
Accepted in revised form 2 November 2010
Available online 12 November 2010

Keywords:
aqueous humour outflow resistance
intraocular pressure
Schlemm's canal
giant vacuole
endothelial transport
cellular biomechanics

ABSTRACT

Aqueous humour transport across the inner wall endothelium of Schlemm's canal likely involves flow through giant vacuoles and pores, but the mechanics of how these structures form and how they influence the regulation of intraocular pressure (IOP) are not well understood. In this study, we developed an in vitro model of giant vacuole formation in human Schlemm's canal endothelial cells (HSCECs) perfused in the basal-to-apical direction (i.e., the direction that flow crosses the inner wall in vivo) under controlled pressure drops (2 or 6 mmHg). The system was mounted on a confocal microscope for time-lapse en face imaging, and cells were stained with calcein, a fluorescent vital dye. At the onset of perfusion, elliptical void regions appeared within an otherwise uniformly stained cytoplasm, and 3-dimensional reconstructions revealed that these voids were dome-like outpouchings of the cell to form *giant vacuole-like structures* or *GVLs* that reproduced the classic "signet ring" appearance of true giant vacuoles. Increasing pressure drop from 2 to 6 mmHg increased GVL height (14 ± 4 vs. 21 ± 7 μm, $p < 0.0001$) and endothelial hydraulic conductivity (1.15 ± 0.04 vs. 2.11 ± 0.49 μl min^{-1} mmHg^{-1} cm^{-2}; $p < 0.001$), but there was significant variability in the GVL response to pressure between cell lines isolated from different donors. During perfusion, GVLs were observed "migrating" and agglomerating about the cell layer and often collapsed despite maintaining the same pressure drop. GVL formation was also observed in human umbilical vein and porcine aortic endothelial cells, suggesting that giant vacuole formation is not a unique property of Schlemm's canal cells. However, in these other cell types, GVLs were rarely observed "migrating" or contracting during perfusion, suggesting that Schlemm's canal endothelial cells may be better adapted to withstand basal-to-apical directed pressure gradients. In conclusion, we have established an in vitro model system to study giant vacuole dynamics, and we have demonstrated that this system reproduces key aspects of giant vacuole morphology and behaviour. This model offers promising opportunities to investigate the role of endothelial cell biomechanics in the regulation of intraocular pressure in normal and glaucomatous eyes.

1. Introduction

The bulk of aqueous humour outflow resistance is generated in the vicinity of the inner wall endothelium of Schlemm's canal (Ethier et al., 1995; Grant, 1963; Mäepea and Bill, 1992), and elevated outflow resistance is the cause of ocular hypertension associated with primary open-angle glaucoma (Grant, 1951). While the mechanism by which the inner wall regulates outflow resistance generation remains unknown, virtually all trabecular outflow must cross the inner wall endothelium as it drains from the eye. The pathway of aqueous humour transport across the inner wall has been a matter of long-standing debate, but it is now widely regarded that aqueous humour passes through giant vacuoles and associated transendothelial pores to enter Schlemm's canal (Johnson and Erickson, 2000; Overby, 2011). Giant vacuoles and pores may likely be involved in the regulation of aqueous humour outflow resistance, but we know little about the mechanics governing the formation of either of these structures.

Giant vacuoles are outpouchings of Schlemm's canal endothelial cells that bulge into the canal lumen, leaving a fluid-filled cavity between the cell and the underlying basement membrane (Garron et al., 1958; Holmberg, 1959) (Fig. 1). Despite the term "vacuole" and their typical intracytoplasmic "signet ring" appearance on electron micrographs (Garron et al., 1958), the giant vacuole cavity is

* Corresponding author. Imperial College London, Department of Bioengineering, South Kensington Campus, Royal School of Mines Building, Room 4.33, London SW7 2AZ, UK. Tel.: +44 (0) 20 7594 6376; fax: +44 (0) 20 7594 9817.
E-mail address: d.overby@imperial.ac.uk (D.R. Overby).

0014-4835/$ – see front matter © 2010 Elsevier Ltd. All rights reserved.
doi:10.1016/j.exer.2010.11.003

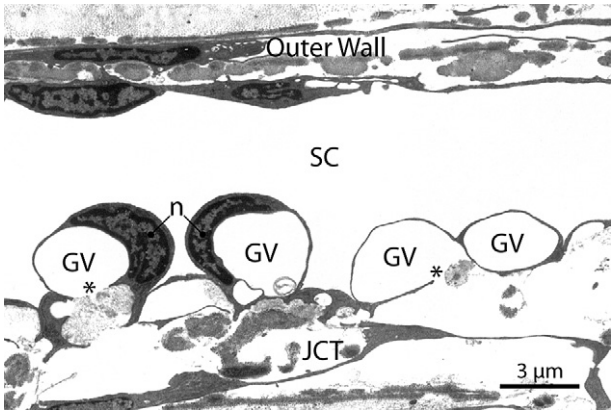

Fig. 1. A transmission electron micrograph showing giant vacuoles (GVs) along the inner wall endothelium of Schlemm's canal (SC). The classic "signet ring" appearance is particularly well exhibited by the second giant vacuole from the left where the cell appears as a thin, continuous lining around the giant vacuole cavity with the nucleus (n) bulging to one side. The first and third giant vacuoles from the left have basal openings or "meshwork pores" (asterisks) where, presumably, aqueous humour enters the giant vacuole cavity from the underlying juxtacanalicular tissue (JCT). Note that the endothelial cells on the outer wall of Schlemm's canal, which is not typically involved in aqueous humour filtration, are flat.

entirely extracellular, and serial sectioning has revealed that most, if not all, giant vacuoles are cellular invaginations that open to the basal side of the endothelium (Grierson and Lee, 1978; Inomata et al., 1972). The size and density of giant vacuoles increase with IOP (Grierson and Lee, 1974, 1975, 1977; Johnstone and Grant, 1973), and giant vacuoles disappear within minutes after IOP is lowered to 0 mmHg (Brilakis and Johnson, 2001), demonstrating that giant vacuoles are pressure- and time-dependent structures. Some giant vacuoles possess one or more micron-sized transendothelial pores that open into the lumen of Schlemm's canal and are thought to provide a passageway for aqueous humour flow across the endothelium (Bill, 1970; Ethier et al., 1998; Grierson and Lee, 1975; Holmberg, 1959, 1965; Inomata et al., 1972; Kayes, 1967; Lee and Grierson, 1975; Tripathi, 1968).

The goal of this study was to develop an in vitro model system to investigate the biomechanics of giant vacuole formation in cultured human Schlemm's canal endothelial cells (HSCECs). Unlike previous in vitro models of giant vacuole formation (Alvarado et al., 2004), our apparatus is mounted on a microscope and allows for time-lapse visualisation of giant vacuole dynamics in living cells during basal-to-apical directed perfusion (i.e., the direction that aqueous humour crosses the inner wall in vivo) while controlling the transendothelial pressure drop. Biomechanical studies of giant vacuole formation are important for understanding how endothelial deformation (e.g., pore formation) contributes to transendothelial fluid drainage across the inner wall of Schlemm's canal. We are motivated by the hypothesis that cell biomechanical processes are centrally involved in generation of aqueous humour outflow resistance and regulation of intraocular pressure, and that alteration of cell biomechanical function is responsible for elevated outflow resistance and ocular hypertension in primary open-angle glaucoma.

2. Materials and methods

2.1. Cell isolation and culture

HSCECs were isolated from ostensibly normal human donor eyes by threading a gelatine-coated suture through Schlemm's canal and culturing for a period of several weeks, following published methods (Stamer et al., 1998). All HSCEC cell lines used in this study were characterised based upon the typical "railroad track" morphology, lack of myocilin induction following exposure to dexamethasone, expression of VE-cadherin, and a threshold transendothelial electrical resistance of 10 Ohms cm^2 in the first passage, following published methods (Heimark et al., 2002; Stamer et al., 2010, 1998; Sumida and Stamer, 2010). HSCECs were cultured in low-glucose Dulbecco's Modified Eagle's Medium (DMEM, Invitrogen) supplemented with 10% foetal bovine serum (FBS), 5 mM L-glutamine, and 1% penicillin/streptomycin at 37 °C and 5% CO_2 in humidified air. HSCECs were sub-cultured prior to confluence by brief exposure to trypsin/EDTA (0.1%/0.02% in PBS), and re-seeded at a ratio of 1:3. Three HSCEC cell lines from donors aged 29, 34 and 71 years (SC56, SC58 and SC52, respectively) were used between passage 3 and 6 for these studies.

Porcine aortic endothelial cells (PAECs) were freshly isolated from the descending thoracic aorta of Landrace-Cross pigs aged 4–6 months (Fresh Tissue Supplies, UK) by digestion in collagenase, following previously described techniques (Bogle et al., 1996; Warboys et al., 2010). PAECs were cultured in DMEM with 10% FBS and antibiotics and sub-cultured prior to confluence, following the same protocol described above for HSCECs. PAECs were used between passage 1 and 2. Human umbilical vein endothelial cells (HUVECs) were purchased from a commercial supplier (Lonza, USA) and cultured in the recommended growth medium. HUVECs were sub-cultured prior to confluence by brief exposure to trypsin/EDTA followed by trypsin neutralisation solution, as recommended by the supplier, and used between passage 3 and 6. All culture chemicals obtained from Sigma (UK) unless otherwise specified.

2.2. Perfusion studies

Two days prior to experiments, HSCECs were seeded at confluence (4.5×10^4 cells/cm^2) onto the bottom-facing surface of a Transwell® permeable filter membrane insert (Corning 3460; 0.4 μm track-etch pore diameter, 12 mm membrane diameter; 4×10^6 pores/cm^2). During seeding, the insert was inverted to expose the bottom-facing filter membrane surface, and a 12 mm folding-skirt Versilic® silicone stopper (VWR, UK) was fit around the insert to act as a retaining collar for the cell suspension. Cells were cultured upright in this configuration for approximately 6 h. The collar was then removed and the insert was placed with the cells facing downwards in a 12-well plate with cell culture medium for an additional 42 h. Preliminary studies showed that this approach yields an approximately uniform distribution of cells across the membrane. PAECs and HUVECs were treated similarly, except they were seeded at a higher density (1.0×10^5 cells/cm^2).

Cells cultured on membrane inserts were used for one of two different experimental protocols: (i) time-lapse studies where living cells were imaged during perfusion; or (ii) perfusion-fixation studies where cells were perfused without time-lapse imaging and then fixed at the same pressure for higher resolution imaging using confocal microscopy. For both protocols, cells were perfused in the basal-to-apical direction at a pressure drop of 2 or 6 mmHg. These pressures were chosen to bound the range of pressure drops expected across the inner wall of Schlemm's canal. For all experiments, cells were cultured for 2 days on the filter membranes prior to perfusion. Our initial work suggested that culture periods greater than 4 days tended to yield less stable perfusion tracings, and extended culture periods (20–30 days) often led to monolayer detachment during perfusion.

2.3. Perfusion studies: time-lapse studies

For time-lapse studies, live cells were loaded with the fluorescent vital dye calcein-AM (2 μM in serum-free DMEM for 30 min at

room temperature; Invitrogen). After loading, the cells were washed in DMEM, and the insert was removed from the culture plate, emptied of medium, and a 10.2 mm folding-skirt Versilic® silicone stopper (VWR, UK) was placed into the upper opening of the insert to create a leak-proof seal and to introduce a small chamber (~0.5 mL) between the top-facing surface of the membrane and the silicone stopper. Prior to placing the silicon stopper into the insert, a 21G needle was threaded through the stopper to shunt any pressure spikes that would otherwise damage the endothelial cell layer. A second needle was then threaded through the stopper, and the chamber between the membrane and stopper was filled with CO_2-independent serum-free perfusion medium (25 mM HEPES in DMEM, Invitrogen). The insert was placed in a well containing perfusion medium, and the cells were allowed to equilibrate for 30 min.

Immediately prior to perfusion, the membrane insert was placed into a customised membrane insert adapter (Bioptechs, Pennsylvania, USA) with the cells facing downwards, and the adapter was mounted on a 35 mm cover glass-bottomed dish that was filled with perfusion medium (Fig. 2A,B). Importantly, the adapter allowed control over the height of the filter membrane so that the cells may be positioned within the working distance of an inverted microscope objective. For HSCECs and PAECs, the adapter was placed on the stage of an inverted confocal microscope (TCS SP5, Leica, UK) that was contained within a temperature-controlled chamber set to 37 °C. For HUVECs, the adapter was placed on the stage of an inverted epifluorescence microscope (TE-2000E, Nikon, USA) with a temperature-controlled stage (Delta-T, Bioptechs) set to 37 °C.

For perfusion, one of the needles that were threaded through the silicone stopper was connected to a computerised perfusion system (Fig. 2A). The second needle was used to backfill the system and to flush bubbles; this needle was removed prior to perfusion. The perfusion system was adapted from a previously described system (Overby et al., 2002). Briefly, it consists of a computer-controlled syringe pump that adjusts the flow rate (Q) across the cell layer to maintain a user-defined pressure drop (ΔP; 2 or 6 mmHg), while continuously recording hydraulic conductivity ($L_p = Q/(\Delta P \times A)$, where A is the membrane area). All measures of L_p were corrected to account for the hydraulic resistance of the filter membrane. Typically, the perfusion system converged to the prescribed pressure drop within 5–10 min (Fig. 2C,D), and perfusions lasted for at least 25 min. HSCECs and PAECs were imaged on a confocal microscope with a 20× objective (200× total magnification, 0.3 NA) with 488 nm excitation and a 505–535 nm emission window appropriate for calcein imaging. Images were acquired at multiple locations along the filter (using a motorised x–y stage) at a lower frame rate (~8 min interval), while some selected locations were imaged at a higher frame rate (15 s interval over 10 min). HUVECs were imaged on an epifluorescence microscope with a 20× objective (200× total magnification, 0.45 NA) and appropriate barrier filters, with images acquired once every 30 s for 20 min.

2.4. Perfusion studies: perfusion-fixation studies

For perfusion-fixation studies, HSCECs were cultured and perfused on the bottom-facing surface of filter membrane inserts following the same protocol that was used for the time-lapse

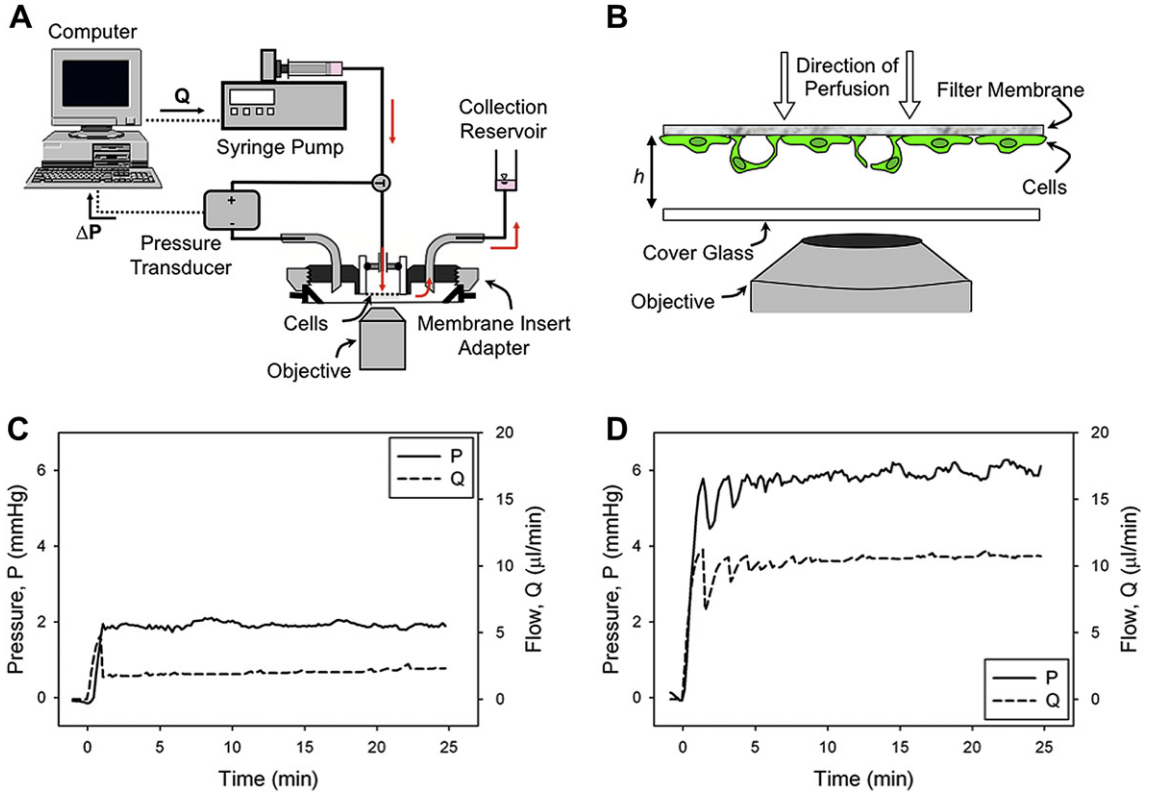

Fig. 2. Diagram of the perfusion system (A) and arrangement of cells on the filter membrane with respect to the microscope objective (B). The flow rate, Q, of perfusion medium across the cell layer is set by a computer-controlled syringe pump that adjusts Q to maintain a user-defined pressure drop, ΔP. The cells are cultured on the bottom-facing surface of a filter membrane with flow (red arrows in panel A) crossing the cell layer in the basal-to-apical direction. The distance, h, between the cells and cover glass can be adjusted using the membrane insert adapter to position the cells within the working distance of the microscope objective. Panels C and D show representative pressure (solid curve; left axis) and flow (dashed curve; right axis) tracings for perfusions at a constant pressure of 2 and 6 mmHg. Note that the perfusion system reaches steady state within 5 min.

studies, with the exception that the cells were not loaded with vital dye. After 25 min of perfusion in the basal-to-apical direction at a pressure drop of 2 or 6 mmHg, the medium contained in the chamber between the top-facing surface of the filter membrane and the silicone stopper was exchanged with 2.5% glutaraldehyde and 2.0% paraformaldehyde in PBS (TAAB Laboratories Equipment, UK). The exchange was controlled using a second bi-directional syringe pump connected to the chamber through two additional 21G needles that were threaded through the silicone stopper prior to the start of the perfusion; the heights of the needle tips were staggered to promote better mixing. During the exchange, the flow rate of the bi-directional syringe pump was set to 200 μl/min while the first "perfusion" syringe pump continued to maintain the same user-defined pressure drop, which typically never fluctuated more than 0.5 mmHg from the target. After 15–20 min, the bi-directional syringe pump was stopped, and perfusion with fixative continued for an additional 30 min at the same pressure. The perfusion was then stopped and the membrane insert was removed from the adapter and immersed in fixative for 30 min.

For fluorescence imaging, HSCECs were permeabilised in Triton ×-100 (0.1% in PBS) for 5 min and then stained with phalloidin-conjugated AlexaFlour-488 (1:40 in PBS, Invitrogen) for 20 min. Confocal z-stacks were acquired using a 63× objective (630× total magnification, 1.30 NA, 488/505–535 nm) through the entire thickness of the cell layer (0.2 μm step size). These images included fluorescent signals from phalloidin-labelled F-actin as well as auto-fluorescence induced by the glutaraldehyde fixation, which in combination yielded a fluorescent signal that delimited the cytoplasm of cells. Cells exhibiting uniform cytoplasmic fluorescence were selected for 3-dimensional reconstructions that were rendered from confocal z-stacks using Volocity® software (PerkinElmer Inc., Massachusetts, USA).

3. Results

Cells were examined for confluency immediately prior to perfusion. HSCECs appeared spindle-shaped with a length and width of approximately 100–300 and 15–30 μm, respectively, while PAECs and HUVECs were more cobblestone-like with a length and width of approximately 30 and 20 μm, respectively. In time-lapse studies at the onset of perfusion, elliptical void regions appeared within the otherwise uniformly stained cytoplasm in all cell types examined (Fig. 3). These void regions spanned a broad range in size from 5 μm in length to upwards of 100 μm and appeared to be associated with large cellular deformations. Importantly, this occurred without leakage of calcein dye elsewhere in the same cells, indicating that the void regions were not associated with rupture of the plasma membrane.

To visualise the morphology of the void regions, we created 3-dimensional reconstructions of confocal z-stack images of the F-actin architecture in perfusion-fixed HSCECs. These reconstructions revealed that the void regions were sites of apical cell displacement into thin dome-like structures that enclosed an extracellular ellipsoidal cavity extending along the long axis of individual cells (Fig. 4). Computer-generated vertical cross-sections typically revealed a continuous cellular lining about the entire cavity, including along its base (Fig. 4B), which is consistent with the classic "signet ring" appearance that was originally attributed to true giant vacuoles along the inner wall of Schlemm's canal (Garron et al., 1958). A basal opening or "meshwork pore" (Grierson and Lee, 1978) was occasionally observed (Fig. 4C), which is presumably the site where perfusion fluid enters the cavity from below. We now refer to the void regions as *giant vacuole-like structures* or *GVLs* on account of their similarity to, but also to distinguish them from, true giant vacuoles observed along the inner wall in situ.

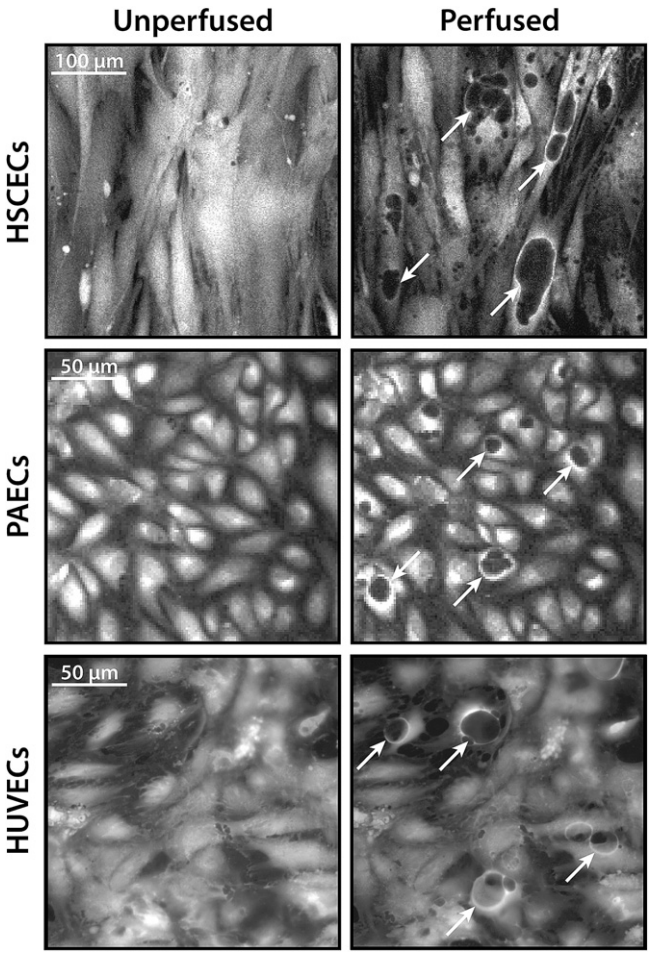

Fig. 3. Elliptical void regions (arrows) appear within the otherwise uniformly stained cytoplasm of living cells during basal-to-apical directed perfusion of HSCECs (top row), PAECs (middle row), or HUVECs (bottom row). The left column of images shows cells prior to perfusion, while the right column shows the same cells after approximately 20 min of perfusion at a pressure drop of 6 mmHg in the basal-to-apical direction. Cells were stained with calcein-AM. Note that HSCECs are intrinsically larger and are therefore displayed at a lower magnification to show approximately the same number of cells per field. The HSCEC cells shown in the top row of images are the same as those shown in the top row of Fig. 8.

We next examined how GVL dimensions depended upon pressure drop across the cell layer, focussing on HSCECs at 2 vs. 6 mmHg. Within an individual cell line (SC52), GVL dimensions (mean ± SD) at 2 mmHg were 45 ± 21, 26 ± 8 and 14 ± 4 μm (length, width, and height; $N = 40$ GVLs over 3 experiments), while at 6 mmHg the same dimensions were significantly larger at 69 ± 24, 33 ± 8 and 21 ± 7 μm ($N = 46$ GVLs over 4 experiments; $p < 0.0001$ for all cases, unpaired Student's *t*-test). Approximating the GVL cavity as an ellipsoid and using standard formulae (Xu et al., 2009), we estimate that the GVL surface area changes 2-fold between 2 mmHg (2590 ± 1740 μm^2; $N = 40$) and 6 mmHg (5100 ± 2380 μm^2; $N = 46$, $p < 0.0001$). The minimum thickness of the cell comprising the wall of the GVL cavity was smaller at 6 mmHg (1.7 ± 0.7 μm; $N = 43$) compared to 2 mmHg (2.4 ± 1.6 μm; $N = 36$; $p < 0.02$). Thus, increasing pressure drop lead to an enlargement of the GVL cavity, expansion of cell surface area, and thinning of the cell comprising the GVL wall (Fig. 5). Moreover, the number of GVLs seen within each image frame appeared to increase with pressure (Fig. 6), although we did not rigorously quantify this metric.

Perhaps the most striking finding, however, was the variability in the GVL response to pressure between different cell lines. In cell

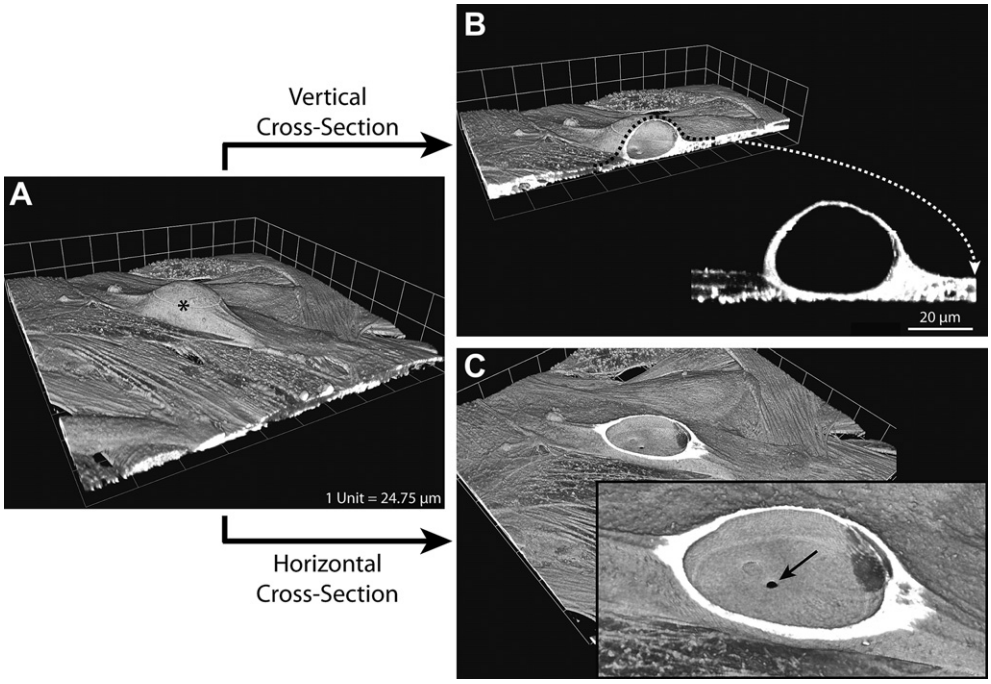

Fig. 4. Three-dimensional confocal reconstruction of a giant vacuole-like structure (GVL) in an HSCEC layer that was perfusion fixed at a pressure drop of 6 mmHg in the basal-to-apical direction (cell line SC52, passage 5). The surface rendering is shown in panel A, with the GVL indicated by an asterisk. A computer-generated vertical cross-section through the GVL (B) reveals a dome-like elliptical cavity with a cellular lining about its entire circumference, including along its base, consistent with the classic "signet ring" appearance attributed to giant vacuoles (cf. Fig. 1). A horizontal cross-section through the GVL reveals that the base of the GVL cavity contains a small opening or "meshwork pore" (~3.5 µm diameter) that is presumably the site where perfusion fluid enters the GVL cavity from below. Cells were glutaraldehyde-fixed to induce auto-fluorescence and stained using phalloidin to label F-actin.

line SC52, GVLs were observed at both 2 and 6 mmHg, and GVLs increased in size and number with increasing pressure. In contrast, GVLs in cell lines SC56 and SC58 were virtually absent at 2 mmHg, and while some GVLs were observed at 6 mmHg, these tended to be smaller and less numerous than those observed in SC52 (Fig. 6). This behaviour was consistent in at least 6 experiments for each cell line. These data demonstrate that GVLs are pressure-dependent structures, however there exists large variability in the pressure response between cell lines isolated from different donors.

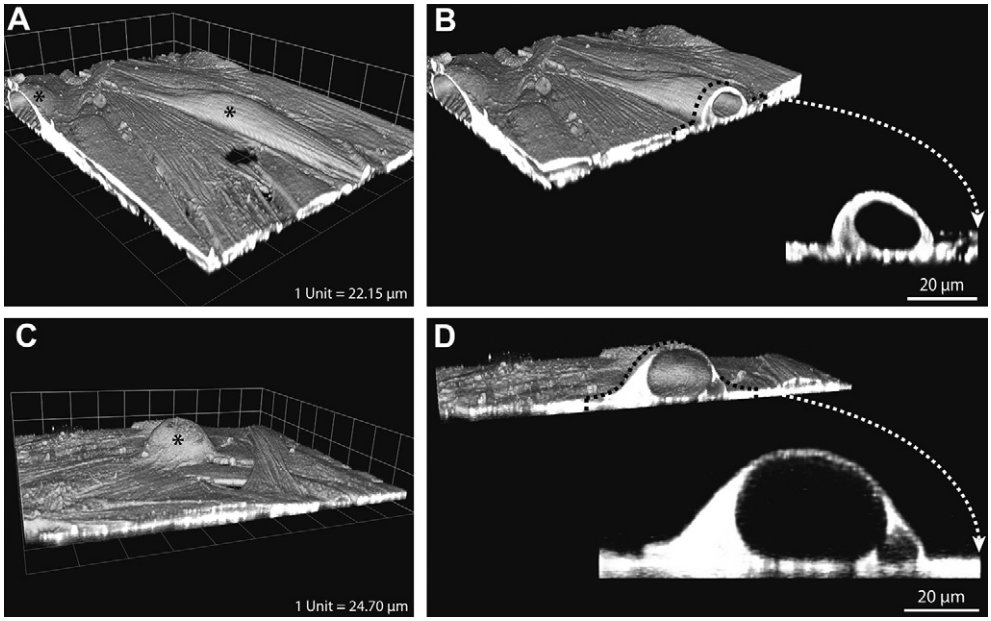

Fig. 5. Three-dimensional confocal reconstructions of giant vacuole-like structures (GVLs) in HSCEC layers that were perfusion fixed at a pressure drop of 2 mmHg (panels A, B) or 6 mmHg (panels C, D). Surface renderings are shown in panels A and C, with GVLs indicated by asterisks. Vertical cross-sections through the same GVLs (panels B and D) reveal the classic "signet ring" appearance, with a continuous cellular lining about the entire GVL cavity (cf. Fig. 1). Note that the insets in panels B and D are presented at the same magnification to demonstrate that GVL size increases with increasing pressure drop, with obvious thinning of the cellular lining with increasing pressure. GVLs were obtained from cell line SC52, passage 4 (panels C, D) and 5 (panels A, B), and the cells were glutaraldehyde-fixed to induce auto-fluorescence and stained with phalloidin to label F-actin.

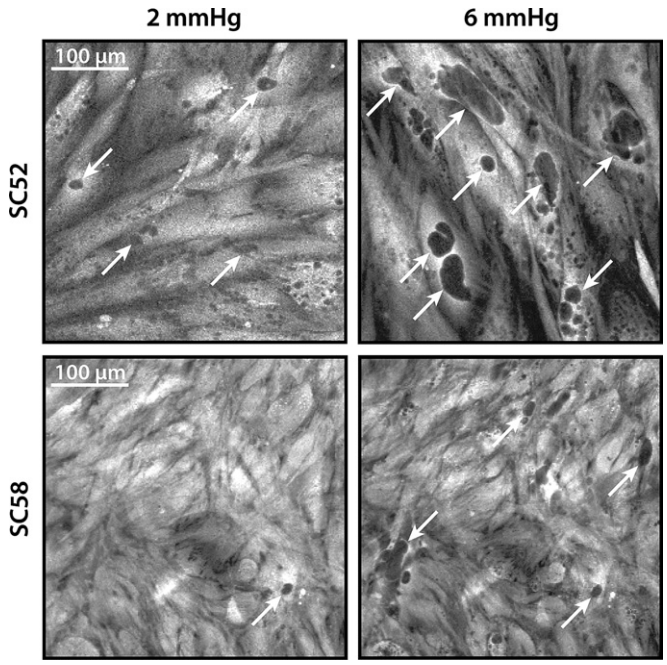

Fig. 6. The size and number of giant vacuole-like structures (GVLs; arrows) increases with increasing pressure drop, but there is a large variability in the pressure response between individual cell lines. Cell line SC52 (71-year-old donor, top row) shows several GVLs at both 2 mmHg (left column) and 6 mmHg (right column) after approximately 20 min of perfusion. However, SC58 (34 year-old donor, bottom row) shows very few GVLs at 2 mmHg, and those at 6 mmHg are smaller and less numerous than those observed in SC52. All panels are presented at the same magnification. Images of SC52 were obtained from different experiments.

Exemplar tracings of L_p measured in the basal-to-apical direction for HSCEC layers are shown in Fig. 7A. L_p measurements typically stabilised within minutes, and maintained a nearly constant value throughout perfusion. With increasing pressure drop in HSCECs, we observed an approximately two-fold increase in L_p between 2 and 6 mmHg (Fig. 7B) that was highly significant ($p < 0.001$, $N = 7$ and 8, respectively; pooling SC52 and SC58). Note that our values of L_p (ranging from 1.08 to 2.98 μl min^{-1} mmHg^{-1} cm^{-2}) are consistent with, although somewhat smaller than, prior reports of L_p in HSCECs (5.23 ± 0.80 μl min^{-1} mmHg^{-1} cm^{-2}) measured in the basal-to-apical direction at 4.5 mmHg (Alvarado et al., 2004). Cell line SC52 tended to yield larger values of L_p at each pressure compared to SC58, but these differences did not achieve statistical significance ($p > 0.3$; $N = 6$ and $N = 3$ for SC52 and SC58, respectively). Throughout perfusion, the cell layer always appeared to remain intact without any sudden increases in L_p that would indicate a sudden loss or detachment of the cell layer. In other words, for all 12 of the time-lapse perfusion experiments used in this study with cell layers imaged over 61 fields of view, we did not observe a single case where a cell was seen detaching from the filter membrane during perfusion. PAECs exhibited similar values of L_p as HSCECs, but with fewer PAEC experiments we were unable to detect any significant change in L_p with increasing pressure (1.32 ± 0.19 vs. 1.53 ± 0.26 μl min^{-1} mmHg^{-1} cm^{-2} for 2 vs. 6 mmHg, respectively; $p = 0.33$, $N = 3$). Note that all values of L_p were measured in the basal-to-apical direction.

By time-lapse imaging, we were able to more closely examine the dynamic events involved in GVL formation (Fig. 8). In HSCECs, we observed at least two populations of GVLs: smaller GVLs (5–15 μm) that were more circular and often appeared in clusters, and larger GVLs (15–100 μm) that were more elliptical with their major axis oriented along the length of the cell. Smaller GVLs were dynamic, forming and disappearing over minutes, often vigorously as if these structures were rapidly bubbling underneath the cell. In some cases, agglomeration of smaller GVLs appeared to give rise to larger GVLs that were often observed "migrating" about the cell layer. While there was a general tendency for GVL size to increase throughout perfusion, occasional decreases in size were observed when larger GVLs appeared to collapse and smaller GVLs disappeared altogether, despite maintaining a constant pressure drop (Fig. 8). This dynamic behaviour was more pronounced at 6 compared to 2 mmHg (cf. Supplemental Movies 1 and 2).

Supplementary videos related to this article can be found at doi:10.1016/j.exer.2010.11.003.

The dynamic behaviour of GVLs observed in HSCECs was in contrast to the rather static behaviour observed in PAECs and HUVECs. While both small and large GVLs were observed in these other cell types, smaller GVLs did not appear to be as clustered or as dynamic as in HSCECs, and larger GVLs were rarely observed to collapse or change shape (Fig. 8; Supplemental Movie 3). GVLs also appeared to be more circular in PAECs and in HUVECs compared to those observed in HSCECs, which may be attributed to differences between the cobblestone versus spindle-shaped morphologies of these different cell types. Overall, these data demonstrate that GVLs may form in endothelial cell types other than HSCECs in response to basal-to-apical directed pressure gradients, but their dynamic behaviour in HSCECs appears to be unique when compared to PAECs and HUVECs.

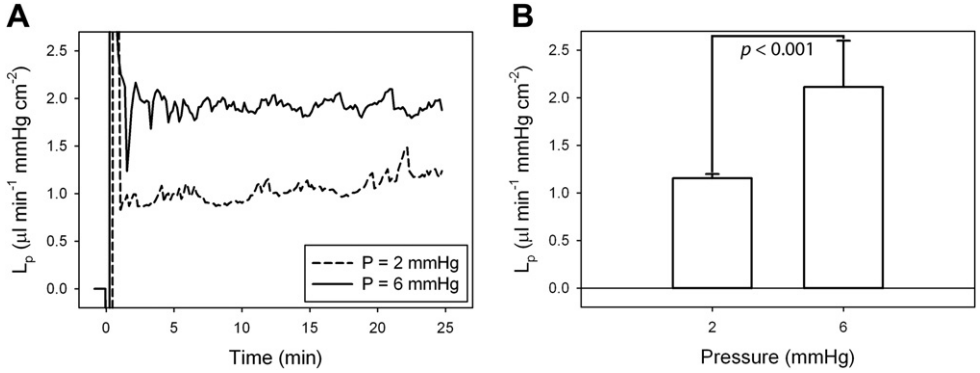

Fig. 7. Representative tracings (panel A, cell line SC58) and aggregate values (panel B, cell lines SC52 and SC58; mean ± SD) of hydraulic conductivity, L_p (μl min^{-1} mmHg^{-1} cm^{-2}), within HSCEC layers at a pressure drop of 2 or 6 mmHg. L_p increased almost two-fold between 2 and 6 mmHg ($p < 0.001$; $N = 7$ or 8). Note that L_p values account for the hydraulic resistance of the filter membrane. Tracings shown in panel A are taken from the same experiments used to produce the pressure and flow tracings shown in Fig. 2C and D.

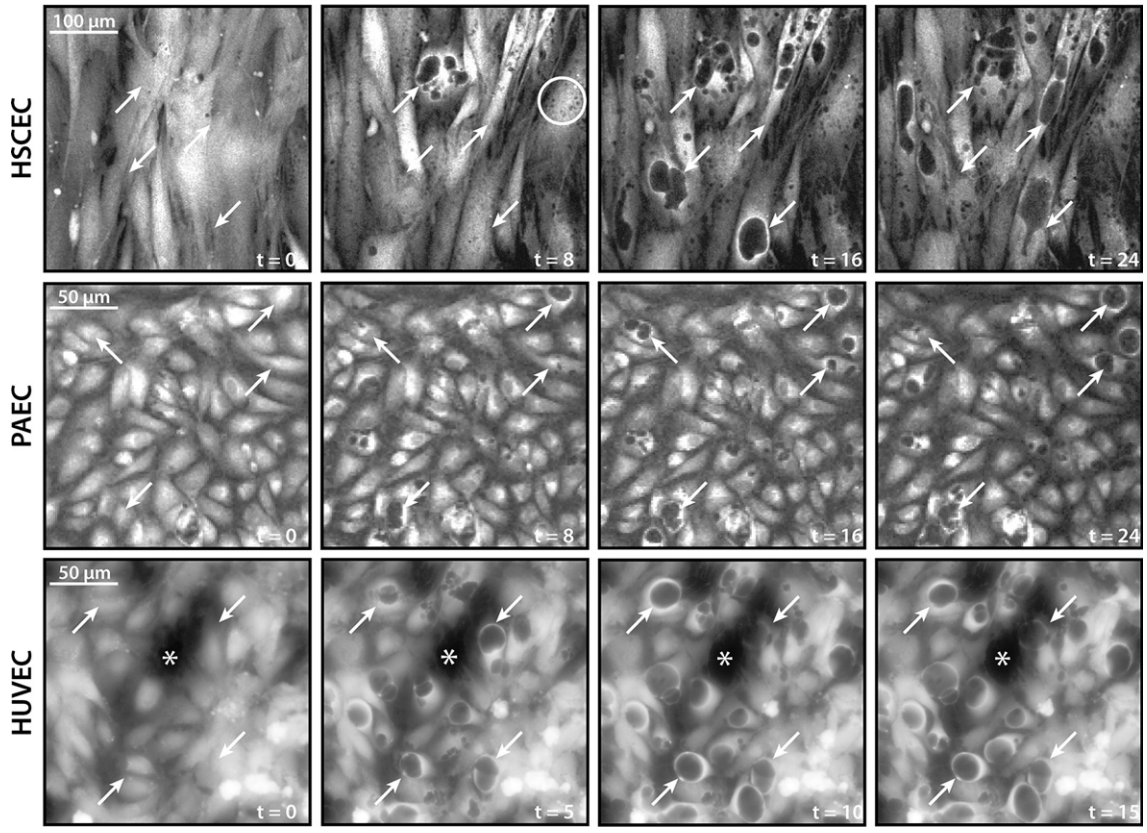

Fig. 8. Time-lapse images of giant vacuole-like structures (GVLs; arrows) forming during basal-to-apical directed perfusion of HSCECs (SC52; top row), PAECs (middle row) and HUVECs (bottom row) at a pressure drop of 6 mmHg. In all cell types, GVL size tended to increase throughout the perfusion, however in HSCECs, GVLs were often observed "migrating" about the cell layer or collapsing despite maintaining the same pressure drop. In contrast, GVLs in PAECs and HUVECs tended to be stationary without contracting during perfusion. The region circled in the second HSCEC cell image identifies a cluster of smaller GVLs that were highly dynamic and can be seen throughout the cell layer (cf. Supplemental Movies). The time of image acquisition (in minutes) after the start of perfusion is indicated at the lower right corner of each frame. Note that GVL formation occurs despite relatively large discontinuities in the cell layer (e.g., the gap indicated by the asterisk in HUVEC images), which is a beneficial consequence of using track-etch filter membranes, as described in the Discussion. Cells were stained with calcein-AM, and HSCECs are presented at a lower magnification on account of their larger cell size.

Supplementary video related to this article can be found at doi:10.1016/j.exer.2010.11.003.

4. Discussion

We hypothesise that Schlemm's canal endothelial cells are centrally involved in the generation of aqueous humour outflow resistance and the regulation of IOP, and that these cells contribute to elevated outflow resistance that leads to ocular hypertension in glaucoma. To better understand how this endothelium may be involved in outflow resistance generation, we developed an experimental system to perfuse human Schlemm's canal endothelial cells (HSCECs) in the basal-to-apical direction under controlled pressure drops, while simultaneously visualising cellular deformation by time-lapse confocal microscopy. Perfusion in the basal-to-apical direction was important to reproduce the direction that aqueous humour crosses the inner wall in vivo. We demonstrate that this approach led to the formation of *giant vacuole-like structures* or *GVLs* that mimicked the morphology and pressure-dependent behaviour of true giant vacuoles, and the formation of GVLs could be visualized in real-time within living cells. This establishes a new in vitro model system that reproduces key functional characteristics of the inner wall endothelium, such that further studies can investigate how Schlemm's canal endothelial cells regulate aqueous humour outflow and outflow resistance generation within a physiologically-relevant biomechanical environment.

Three-dimensional reconstructions confirmed that GVLs were morphologically similar to true giant vacuoles observed in situ. A defining feature of true giant vacuoles is their "signet ring" appearance on micrograph sections (Garron et al., 1958), where a continuous cellular lining is often seen about the entire perimeter of the giant vacuole cavity, with the nucleus usually bulging to one side (cf. Figs. 1, 4B and 5B,D). This is consistent with the fact that giant vacuoles are actually invaginations of the basal cell surface that are surrounded by cell on all sides except where the small mouth of the cavity (known as the "meshwork pore" (Grierson and Lee, 1978); cf. Figs. 1 and 4C) opens into the medium below the cell. Importantly, this demonstrates that giant vacuole formation is not a simple process of an endothelial cell peeling from its basal lamina and displacing apically, as occurs during blister formation (Blackshear et al., 1982), but rather suggests a complex infolding of the cell itself where the cavity develops from the meshwork pore as if a finger of fluid were being pushed through the cell body. The fact that GVLs exhibited the classic "signet ring" appearance and, in some cases, "meshwork pores" suggest that fundamental aspects of giant vacuole formation have been reproduced in this in vitro model system.

The in vitro model system was also able to reproduce the pressure-dependence of true giant vacuoles, and our data suggest that HSCECs experience extreme deformation during giant vacuole formation. It is well recognised that true giant vacuoles become larger with increasing IOP (Grierson and Lee, 1974, 1975; Johnstone and Grant, 1973), with measurements obtained in rhesus monkey

eyes revealing a 50% increase in giant vacuole width and a 37% increase in length between 8 and 15 mmHg (Grierson and Lee, 1977). These data are comparable to the changes in GVL dimensions observed in the current study between 2 and 6 mmHg (27 ± 11% and 53 ± 31% for width and length, respectively, for SC52). However, the absolute dimensions of the in vitro GVLs were much larger than those measured in situ (discussed further below). As the GVL cavity expands with increasing pressure, the cell comprising the wall of the GVL cavity experiences large deformation, as evidenced by a 2-fold increase in surface area coincident with a 30% reduction in cell thickness (for cell line SC52). It is not clear how these cells withstand such large deformation, particularly when the plasma membrane is thought to rupture when it is stretched by 5% or less (Needham and Nunn, 1990). However, we point out that many cells possess a large reservoir of excess membrane stored in ruffles, folds, or vesicles (Lee and Schmid-Schönbein, 1995; Raucher and Sheetz, 1999) that allow the cell to rapidly change shape without altering the total membrane surface area. A recent review presents a more detailed discussion of the deformation involved in giant vacuole formation (Overby, 2011).

Despite exhibiting a similar pressure dependence, the absolute dimensions of GVLs in the current study were much larger than the dimensions of true giant vacuoles, which are reported to have a width of 2.4 ± 0.3 μm and length of 5.2 ± 0.3 μm in rhesus monkeys at 15 mmHg IOP (Grierson and Lee, 1977). In contrast, even at pressure drops as low as 2 mmHg, the length and width of GVLs measured in the current study were 45 ± 21 μm and 26 ± 8 μm, respectively, for SC52. There are at least two explanations for this discrepancy. First, because both giant vacuoles and GVLs depend upon pressure, the pressure drop across the in vitro cell layer may have been larger than occurs across the inner wall cells in vivo. This would be the case if in vivo the inner wall cells themselves generate little resistance to aqueous humour outflow. However, the relative absence of GVLs in some cell lines (SC56 and SC58) at 2 mmHg argues against this possibility. Second, the larger GVL dimensions could be due to a larger cell area of HSCECs in vitro compared to their in vivo counterparts. In this study, the projected area of individual HSCECs ($N = 40$; SC52) within a confluent monolayer before perfusion was 5000 ± 1600 μm^2, compared to 408–480 μm^2 as has been previously reported for human inner wall cells in situ (Bill and Svedbergh, 1972; Lütjen-Drecoll and Rohen, 1970). This difference in area would coincide with an approximately 3-fold difference in linear dimensions of GVLs, which would place these values within the upper limits of giant vacuole size reported by Grierson and Lee (1977) for physiologic IOP (maximum width of 10 μm and maximum length of 14 μm at 15 mmHg). Consistent with this notion, cells from SC52, which formed larger and more numerous GVLs at a given pressure, tended to have a larger area than cells from SC56 and SC58 (Fig. 6).

A striking finding from this study was the variable response between different HSCEC cell lines to perfusion pressure in regards to GVL formation. While GVLs were observed at both 2 and 6 mmHg in cell line SC52, cell lines SC56 and SC58 had virtually no GVLs at 2 mmHg and those at 6 mmHg were much smaller and less frequent than in SC52 (Fig. 6). We do not yet understand the reason for such variability, but it could be related to differences in biomechanical properties (e.g., cell stiffness, adhesion strength, or cell size), extracellular matrix deposition, or density of transendothelial pores as are often observed in these cells in situ. Alternatively, it is tempting to speculate that GVL formation may depend upon donor age. Consistent with this notion, cell line SC52, which demonstrated the greatest potential to form GVLs at either pressure, was isolated from a 71-year-old donor, whereas SC56 and SC58 lines were isolated from 29 to 34-year-old donors, respectively. This suggests that age-related changes in cell biomechanical properties, extracellular matrix deposition or pore formation may influence giant vacuole formation, with cells from younger eyes possibly better adapted to withstand basal-to-apical directed pressure gradients. We point out, however, that this suggestion is in direct conflict with reports describing a decline in giant vacuole counts with age (Boldea et al., 2001; McMenamin et al., 1986), although this could be partly attributed to an age-related decline in the number of inner wall cells themselves (Grierson et al., 1984) or an age-related decline in aqueous humour production (Gabelt and Kaufman, 2005). Regardless, the significant differences observed between cell lines are suggestive of significant biomechanical variability between donors that requires further characterisation, particularly for future studies that aim to compare between glaucomatous and normal cell lines.

In this study, we observed GVL formation during perfusion of PAECs and HUVECs, cells which are derived from large arterial and venous endothelia, respectively, and experience very different biomechanical stimuli (i.e., shear and stretch) in vivo compared to Schlemm's canal endothelia (i.e., basal-to-apical directed pressure drop). The formation of GVLs in PAECs and HUVECs suggests that giant vacuole formation is not a unique property of Schlemm's canal endothelia per se, but rather a general response of a broader class of endothelial cells to basal-to-apical directed pressure gradients. This is consistent with the fact that giant vacuoles are also observed in dural sinus endothelial cells located within the arachnoid villi (Levine et al., 1982), where the basal-to-apical directed flow of cerebrospinal fluid is similar to the flow of aqueous humour across the inner wall of Schlemm's canal (Tripathi and Tripathi, 1974).

Interesting differences between cell types were observed in the dynamic processes involved in GVL formation. In HSCECs, we often observed GVLs "migrating" about the cell layer and larger GVLs forming from the agglomeration of smaller clustered GVLs. These smaller GVLs appeared to rapidly form and disappear between individual frames, as if part of a vigorous bubbling process, while larger GVLs tended to grow more slowly throughout the perfusion. Importantly, rapid decreases in GVL size were often observed, indicating collapse of the GVL despite maintaining the same pressure drop. This was in sharp contrast to the relatively static behaviour observed in PAECs and HUVECs, where GVLs tended to maintain their shape once formed and were rarely seen "migrating" or collapsing during perfusion. These differences could be attributed to the differences in morphology (spindle-shaped HSCECs vs. cobblestone-like PAECs and HUVECs) or differences in behaviour between cells isolated from large vessel and micro-vascular endothelia. Alternatively, these data may suggest that HSCECs are particularly well adapted to withstand basal-to-apical directed pressure gradients, with the ability to contract against an applied load or to rapidly release the fluid contents of the GVL cavity. Interestingly, the latter possibility would be consistent with the known pore-forming ability of these cells in vivo.

Previous investigators have already established that giant vacuole-like structures form in endothelia during in vitro perfusion in the basal-to-apical direction, but unlike the current study, prior work was limited to perfusion-fixed samples. Using cells isolated from human arachnoid granulations or explants of the granulations themselves, which exhibit giant vacuoles in situ, Grzybowski and colleagues demonstrated the formation of vacuole-like structures following basal-to-apical directed transendothelial perfusion (Glimcher et al., 2008; Grzybowski et al., 2006). Using Schlemm's canal endothelial cells, Alvarado and colleagues described the formation of giant vacuole-like structures that were observed after perfusion-fixation in the basal-to-apical, but not in the apical-to-basal, direction (Alvarado et al., 2004). Consistent with our current findings, they (Alvarado et al., 2004) reported that the aggregate

vacuole area, as measured by scanning electron microscopy, increased in a time- and pressure-dependent manner. However, beyond 30–40 min of perfusion or for perfusion pressures greater than 3.0–4.5 mmHg, they (Alvarado et al., 2004) observed a sharp decline in vacuole area that they attributed to a loss of monolayer integrity. We do not completely understand why HSCECs were able to withstand larger perfusion pressures in our setup (up to 6 mmHg for $>$ 30 min), but these differences may be attributable to methodological differences in the preparation technique (e.g., a culture time of 2 days vs. 20–30 days (Alvarado et al., 2004)) or to technical differences in the choice of the filter membrane itself. In our hands, we were unable to achieve vacuole formation in HSCECs cultured on the same Millipore-HA filters following the techniques described by Alvarado (Alvarado et al., 2004). Our studies instead found multiple cell layers that often detached from the filter membrane at the onset of basal-to-apical directed perfusion, and for these reasons we chose instead to use track-etch filters.

A key design feature of our perfusion apparatus is the choice of the track-etch filter membrane that serves as the underlying support for the endothelial cells. Track-etch filters contain nearly perfect cylindrical pores that pass straight through the thickness of an otherwise impermeable material, and the pores themselves do not intercommunicate, such that flow cannot pass laterally along the filter. This is in stark contrast to fibrous filters, such as the Millipore-HA filters used by Alvarado et al. (2004), which have a fibre matrix architecture that allows flow to percolate laterally throughout. This architectural difference between track-etch and fibrous filters becomes very important when perfusing endothelial cells in vitro that typically contain unavoidable gaps or imperfections at sites where full confluency is not reached or where cell–cell junctions have not fully matured (e.g., the gap shown within the HUVEC layer in Fig. 8), which is a well-recognised limitation for most in vitro endothelial transport studies (Albelda et al., 1988; Michel and Curry, 1999). With a fibrous filter, flow would channel through these gaps, with lateral flow acting as a shunt to reduce the pressure drop across the neighbouring cells. Track-etch filters, in contrast, prevent this shunting effect by disallowing lateral flow, so that the pressure drop across the cell layer is maintained despite the presence of local endothelial gaps or imperfections. Therefore, track-etch filter membranes appear to be more suitable for our application because they provide more robust control over the transcellular pressure drop and are less sensitive to the gaps or imperfections commonly encountered with in vitro endothelial perfusion studies.

With increasing pressure drop, we measured a nearly two-fold increase in L_p in HSCECs perfused in the basal-to-apical direction. Similar pressure-induced increases in L_p have been reported in bovine aortic endothelial cells (Tarbell et al., 1999) and bovine lung micro-vascular endothelial cells (Dull et al., 2007), which was attributed to a nitric oxide (NO)-dependent mechanism induced by enhanced flow and elevated shear stress within the intercellular cleft. We did not explicitly examine the mechanism of increasing L_p in response to elevated pressure drop in HSCECs. Although it is possible that similar NO-dependent factors are involved, those previous studies (Dull et al., 2007; Tarbell et al., 1999) perfused endothelial layers in the apical-to-basal direction (i.e., the opposite direction used in the current study) where L_p values are typically 10-fold smaller than in the basal-to-apical direction (Alvarado et al., 2004). It seems certain, however, that the pressure-induced increase in L_p is the result of increased porosity of the endothelium, which may be caused by separation of neighbouring endothelial cells and widening of the paracellular space to create large gaps. Alternatively, the endothelium itself may form micron-sized transendothelial pores, as are observed along the inner wall in situ (Ethier et al., 1998). If HSCECs retain their pore-forming ability in vitro, then the increase in L_p with increasing pressure drop would be consistent with a pressure-induced increase in pore density and/or size, which could be triggered by elevated mechanical strain acting on the endothelial cell as it deforms into a giant vacuole (Overby, 2011). Although our current images provide no evidence for pore formation in HSCECs perfused in vitro, such pores would be very difficult to detect with confocal microscopy due to limitations in optical resolution. Ongoing studies are examining perfusion-fixed cell layers for micron-sized pores using electron microscopy.

In conclusion, we have established an in vitro model of giant vacuole dynamics, and we have demonstrated that this system reproduces key aspects of true giant vacuoles observed along the inner wall endothelium of Schlemm's canal. Because the inner wall is likely a principal component of outflow resistance generation, this model system offers promising new opportunities to investigate how endothelial cell biomechanics, specifically giant vacuole and pore dynamics, are involved in the regulation of IOP and how these contribute to ocular hypertension in glaucoma. Finally, this model system may also be used to screen compounds that affect giant vacuoles or endothelial cell biomechanics as a strategy to identify promising therapeutics to lower IOP for glaucoma therapy.

Acknowledgements

We acknowledge funding support from the Whitaker International Scholars Program (RMP), National Glaucoma Research, a program of the American Health Assistance Foundation (DRO), US National Institutes of Health grants EY018373 (DRO), EY019696 (DRO, WDS), and EY17007 (WDS). We thank Profs. Mark Johnson and Ross Ethier for thoughtful comments and helpful discussions throughout this study and Dr. Thomas Read for providing the giant vacuole image shown in Fig. 1. We thank Dr. Christina Abbott for providing porcine aortic endothelial cells, and the Facility for Imaging by Light Microscopy (FILM) at Imperial College for use of Volocity® software. Finally, we thank Kristin Perkumas for her careful work isolating human Schlemm's canal endothelial cells.

References

Albelda, S.M., Sampson, P.M., Haselton, F.R., McNiff, J.M., Mueller, S.N., Williams, S.K., Fishman, A.P., Levine, E.M., 1988. Permeability characteristics of cultured endothelial cell monolayers. J. Appl. Physiol. 64, 308–322.

Alvarado, J.A., Betanzos, A., Franse-Carman, L., Chen, J., Gonzalez-Mariscal, L., 2004. Endothelia of Schlemm's canal and trabecular meshwork: distinct molecular, functional, and anatomic features. Am. J. Physiol. Cell Physiol. 286, C621–C634.

Bill, A., 1970. Scanning electron microscopic studies of the canal of Schlemm. Exp. Eye Res. 10, 214–218.

Bill, A., Svedbergh, B., 1972. Scanning electron microscopic studies of the trabecular meshwork and the canal of Schlemm–an attempt to localize the main resistance to outflow of aqueous humor in man. Acta Ophthalmol. (Copenh) 50, 295–320.

Blackshear Jr., P.L., Blackshear, G.L., Newell, M.K., Kayser, S.J., Emerson, P.F., 1982. The Localization of Transient Subendothelial Water-Filled Blisters in the in Situ Rabbit Aorta as a Result of Reduction in Pressure. Fluid Dynamics as a Localizing Factor for Atherosclerosis. Springer–Verlag, Heidelberg. 116–128.

Bogle, R.G., Baydoun, A.R., Pearson, J.D., Mann, G.E., 1996. Regulation of l-arginine transport and nitric oxide release in superfused porcine aortic endothelial cells. J. Physiol. 490 (Pt 1), 229–241.

Boldea, R.C., Roy, S., Mermoud, A., 2001. Ageing of Schlemm's canal in non-glaucomatous subjects. Int. Ophthalmol. 24, 67–77.

Brilakis, H.S., Johnson, D.H., 2001. Giant vacuole survival time and implications for aqueous humor outflow. J. Glaucoma 10, 277–283.

Dull, R.O., Mecham, I., McJames, S., 2007. Heparan sulfates mediate pressure-induced increase in lung endothelial hydraulic conductivity via nitric oxide/reactive oxygen species. Am. J. Physiol. Lung Cell Mol. Physiol. 292, L1452–L1458.

Ethier, C.R., Coloma, F.M., de Kater, A.W., Allingham, R.R., 1995. Retroperfusion studies of the aqueous outflow system. Part 2: studies in human eyes. Invest. Ophthalmol. Vis. Sci. 36, 2466–2475.

Ethier, C.R., Coloma, F.M., Sit, A.J., Johnson, M., 1998. Two pore types in the inner-wall endothelium of Schlemm's canal. Invest. Ophthalmol. Vis. Sci. 39, 2041–2048.

Gabelt, B.T., Kaufman, P.L., 2005. Changes in aqueous humor dynamics with age and glaucoma. Prog. Retin. Eye Res. 24, 612–637.

Garron, L.K., Feeney, M.L., Hogan, M.J., McEwen, W.K., 1958. Electron microscopic studies of the human eye. I. Preliminary investigations of the trabeculas. Am. J. Ophthalmol. 46, 27–35.
Glimcher, S.A., Holman, D.W., Lubow, M., Grzybowski, D.M., 2008. Ex vivo model of cerebrospinal fluid outflow across human arachnoid granulations. Invest. Ophthalmol. Vis. Sci. 49, 4721–4728.
Grant, W.M., 1951. Clinical measurements of aqueous outflow. Am. J. Ophthalmol. 34, 1603–1605.
Grant, W.M., 1963. Experimental aqueous perfusion in enucleated human eyes. Arch. Ophthalmol. 69, 783–801.
Grierson, I., Howes, R.C., Wang, Q., 1984. Age-related changes in the canal of Schlemm. Exp. Eye Res. 39, 505–512.
Grierson, I., Lee, W.R., 1974. Changes in the monkey outflow apparatus at graded levels of intraocular pressure: a qualitative analysis by light microscopy and scanning electron microscopy. Exp. Eye Res. 19, 21–33.
Grierson, I., Lee, W.R., 1975. Pressure-induced changes in the ultrastructure of the endothelium lining Schlemm's canal. Am. J. Ophthalmol. 80, 863–884.
Grierson, I., Lee, W.R., 1977. Light microscopic quantitation of the endothelial vacuoles in Schlemm's canal. Am. J. Ophthalmol. 84, 234–246.
Grierson, I., Lee, W.R., 1978. Pressure effects on flow channels in the lining endothelium of Schlemm's canal. A quantitative study by transmission electron microscopy. Acta Ophthalmol. (Copenh) 56, 935–952.
Grzybowski, D.M., Holman, D.W., Katz, S.E., Lubow, M., 2006. In vitro model of cerebrospinal fluid outflow through human arachnoid granulations. Invest. Ophthalmol. Vis. Sci. 47, 3664–3672.
Heimark, R.L., Kaochar, S., Stamer, W.D., 2002. Human Schlemm's canal cells express the endothelial adherens proteins, VE-cadherin and PECAM-1. Curr. Eye Res. 25, 299–308.
Holmberg, A., 1959. The fine structure of the inner wall of Schlemm's canal. Arch. Ophthalmol. 62, 956.
Holmberg, Å, 1965. Schlemm's canal and the trabecular meshwork. An electron microscopic study of the normal structure in man and monkey (*Cercopithecus Aethiops*). Doc. Ophthalmol. 19, 339.
Inomata, H., Bill, A., Smelser, G.K., 1972. Aqueous humor pathways through the trabecular meshwork and into Schlemm's canal in the Cynomolgus monkey (Macaca Irus). An electron microscopic study. Am. J. Ophthalmol. 73, 760–789.
Johnson, M., Erickson, K., 2000. Mechanisms and routes of aqueous humor drainage. In: Albert, D.M., Jakobiec, F.A. (Eds.), Principles and Practices of Ophthalmology. WB Saunders Co., Philadelphia, pp. 2577–2595.
Johnstone, M.A., Grant, W.G., 1973. Pressure-dependent changes in structures of the aqueous outflow system of human and monkey eyes. Am. J. Ophthalmol. 75, 365–383.
Kayes, J., 1967. Pore structure of the inner wall of Schlemm's canal. Invest. Ophthalmol. Vis. Sci. 6, 381.
Lee, W.R., Grierson, I., 1975. Pressure effects on the endothelium of the trabecular wall of Schlemm's canal: a study by scanning electron microscopy. Albrecht Von Graefes Arch. Klin. Exp. Ophthalmol. 196, 255–265.
Lee, J., Schmid-Schönbein, G.W., 1995. Biomechanics of skeletal muscle capillaries: hemodynamic resistance, endothelial distensibility, and pseudopod formation. Ann. Biomed. Eng. 23, 226–246.
Levine, J.E., Povlishock, J.T., Becker, D.P., 1982. The morphological correlates of primate cerebrospinal fluid absorption. Brain Res. 241, 31–41.
Lütjen-Drecoll, E., Rohen, J.W., 1970. Endothelial studies of the Schlemm's canal using silver-impregnation technic. Albrecht Von Graefes Arch. Klin. Exp. Ophthalmol. 180, 249–266.
Mäepea, O., Bill, A., 1992. Pressures in the juxtacanalicular tissue and Schlemm's canal in monkeys. Exp. Eye Res. 54, 879–883.
McMenamin, P.G., Lee, W.R., Aitken, D.A., 1986. Age-related changes in the human outflow apparatus. Ophthalmology 93, 194–209.
Michel, C.C., Curry, F.E., 1999. Microvascular permeability. Physiol. Rev. 79, 703–761.
Needham, D., Nunn, R.S., 1990. Elastic deformation and failure of lipid bilayer membranes containing cholesterol. Biophys. J. 58, 997–1009.
Overby, D., Gong, H., Qiu, G., Freddo, T.F., Johnson, M., 2002. The mechanism of increasing outflow facility during washout in the bovine eye. Invest. Ophthalmol. Vis. Sci. 43, 3455–3464.
Overby, D.R., 2011. The mechanobiology of aqueous humor transport across Schlemm's canal endothelium. In: Nagatomi, J. (Ed.), Mechanobiology Handbook. Taylor & Francis Group, Boca Raton.
Raucher, D., Sheetz, M.P., 1999. Characteristics of a membrane reservoir buffering membrane tension. Biophys. J. 77, 1992–2002.
Stamer, W.D., Piwnica, D., Jolas, T., Carling, R.W., Cornell, C.L., Fliri, H.G., Martos, J.L., Pettit, S.N., Wang, J.W., Woodward, D.F., 2010. Cellular basis for bimatoprost effects on human conventional outflow. Invest. Ophthalmol. Vis. Sci. 51, 5176–5181.
Stamer, W.D., Roberts, B.C., Howell, D.N., Epstein, D.L., 1998. Isolation, culture, and characterization of endothelial cells from Schlemm's canal. Invest. Ophthalmol. Vis. Sci. 39, 1804–1812.
Sumida, G.M., Stamer, W.D., 2010. Sphingosine-1-phosphate enhances cortical actomyosin organization in cultured human Schlemm's canal endothelial cell monolayers. Invest. Ophthalmol. Vis. Sci., doi:10.1167/iovs.10-5391.
Tarbell, J.M., Demaio, L., Zaw, M.M., 1999. Effect of pressure on hydraulic conductivity of endothelial monolayers: role of endothelial cleft shear stress. J. Appl. Physiol. 87, 261–268.
Tripathi, B.J., Tripathi, R.C., 1974. Vacuolar transcellular channels as a drainage pathway for cerebrospinal fluid. J. Physiol. 239, 195–206.
Tripathi, R.C., 1968. Ultrastructure of Schlemm's canal in relation to aqueous outflow. Exp. Eye Res. 7, 335–341.
Warboys, C.M., Eric Berson, R., Mann, G.E., Pearson, J.D., Weinberg, P.D., 2010. Acute and chronic exposure to shear stress have opposite effects on endothelial permeability to macromolecules. Am. J. Physiol. Heart Circ. Physiol. 298, H1850–H1856.
Xu, D., Cui, J., Bansal, R., Hao, X., Liu, J., Chen, W., Peterson, B.S., 2009. The ellipsoidal area ratio: an alternative anisotropy index for diffusion tensor imaging. Magn. Reson. Imaging 27, 311–323.